TRAVELLING WAVE KICKER MAGNETS WITH SHARP RISE AND LESS OVERSHOOT

G. Nassibian[*]

Introduction and Summary

As an alternative to the classical design of travelling wave kicker magnets, a structure with a fairly simple additional feature was developed and investigated. This modification was based on the following considerations.

The shape of the rise of the magnetic field in a travelling wave kicker is determined by two main factors: i) the shape of the applied current pulse, and ii) the propagation characteristics of the magnet structure.

In the PSB kicker system[1], kiloampere pulses with a rise-time of ~ 10 ns are obtained by means of ferrite-loaded pulse steepening lines[2]. Measurements show, however, that pulses with this rise-time are severely distorted as they travel along the various kicker magnets. It was therefore thought worth while to examine whether any improvements might be possible, other than the classical remedies of increasing the number of cells or raising the characteristic impedance.

To this end a typical magnet module (Fig. 1) was measured using RF techniques and its dispersion curve compared to calculations for various possible equivalent circuits.

After concluding that the mutual inductance between cells was a dominant factor, the kicker was modified by adding inductive coupling of opposite sign. This considerably improved the dispersion curve, with a corresponding increase in the phase and group velocities for high frequencies.

Although attenuation still produces some distortion, pulse measurements confirmed that the pulse transmission was substantially improved.

Frequency domain measurements

The characteristics of the magnet used were:

Nominal impedance	25 Ω
Number of cells N	13
Aperture height 2a	70 mm
Aperture width 2b	115 mm
Cell length d	32 mm
Ferrite thickness	26 mm.

In order to measure the propagation constant, two shorting pistons, each fitted with a small coupling loop, were placed at the ends of the kicker. The resonant frequencies corresponding to wavelengths $\lambda = 2Nd/n$, n = 1, 2, 3, were measured, and the process repeated after reducing the distance between pistons by one or more cell lengths. The results are shown in Fig. 2(a) where $\Theta = 360 \, d/\lambda$.
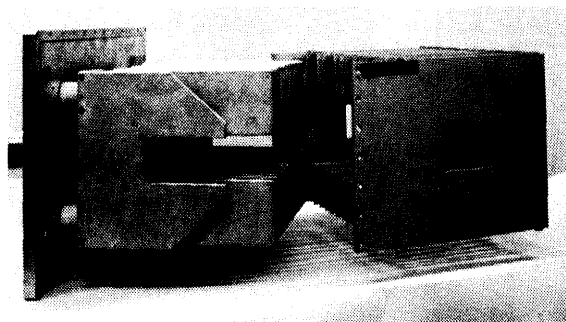
Fig. 1 - Kicker magnet (partially dismantled)

*) PS Division, CERN, Geneva, Switzerland.
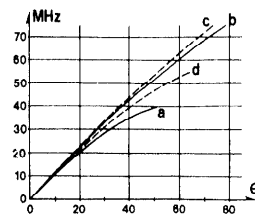
Fig. 2 - Measured dispersion curves
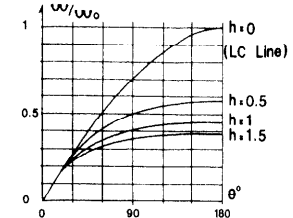
Fig. 3 - Dispersion curves for circuit I

In such a diagram, the slope of a line joining a point on the curve to the origin is proportional to the phase velocity, while the slope of the tangent is proportional to the group velocity.

While the shorting pistons help to overcome the fact that normally the end sections have different inductance (due to fringing of the magnetic field, which they suppress) and different capacity (presence of part of the connections, etc.) they do not necessarily provide perfect end conditions, particularly if there is mutual inductance between cells.

Another difficulty arises from the fact that the kicker is only approximately uniform.

For both these reasons, preference was given to measurements involving as many cells as possible, thus providing some degree of averaging and reducing the relative importance of imperfect end conditions.

While measurement techniques could be refined, the extra work would not be justified unless the precision of construction was increased correspondingly.

Comparison with possible equivalent circuits

Circuit I

The simplest representation of a kicker cell that gives realistic results is the well-known[3-5] circuit I of Fig. 4, where $L_1 \cong \mu_0 bd/a$.

Writing
$$L_2 = hL_1$$
$$\omega_0 = 2(L_1C_2)^{-\frac{1}{2}}$$

and

$$y = \omega/\omega_0$$

the propagation constant is given by
$$\Theta = 2 \arcsin y(1 - 4hy^2)^{-\frac{1}{2}} \qquad (1)$$

and the cut-off by
$$\omega_c = \omega_0(1 + 4h)^{-\frac{1}{2}}$$

The effect of varying L_2 for fixed L_1 and C_2 is shown in Fig. 3.

Fitting (1) to the measured data, we find
$$f_0 = \omega_0/2\pi = 125 \text{ MHz}$$
$$h \cong 1.08$$
$$f_c = \omega_c/2\pi \cong 54 \text{ MHz}$$
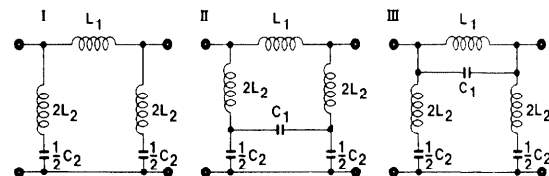
Fig. 4 - Circuit representations

This value of ω_0 is consistent with that which one calculates from the measured values of L_1 and C_2.

Although the fit to the measured data is surprisingly good, careful comparison shows that the measured curve flattens rather faster than (1).

One feature obviously neglected in this circuit is the capacity between consecutive "live" plates. These not only "see" each other to some extent, but are also bridged by ferrite, which because of its high dielectric constant, stores a considerable amount of electrostatic energy.

The resultant capacity cannot be measured statically but can be estimated, taking into account the distribution of electric field across the ferrite.

Circuit II

To try to obtain a better fit with the data, the circuit II of Fig. 4 was next examined. There the assumption is that L_2 has a physical reality, i.e. it arises from the fact that the current, flowing outwards from the live conductor, must pass between ferrites.

Writing $L_2 = kL_1$, $C_1 = nC_2$, one finds that the propagation constant can be put in the form

$$\Theta = 2 \arcsin y \left\{ 1 - 4 \left[k + \frac{n}{1 - 4k(1 + 4n)y^2} \right] y^2 \right\}^{-\frac{1}{2}} . \quad (2)$$

For very small values of y, (2) reduces to (1) with $h = k + n$. This circuit gives an excellent fit to the data, but with a value of n that is implausibly small. This in turn suggests that the major part of L_2 may not be a physical inductance, but simply a circuit representation of the (opposing) mutual inductance between cells.

Modifying the kicker so as to reduce C_1 resulted in some improvement of the dispersion curve, but the change was not large enough to be of practical significance.

Circuit III

We next examine circuit III of Fig. 4, which would be appropriate if L_2 were in fact only a circuit representation of the mutual inductance between cells. Writing $L_2 = kL_1$, $C_1 = nC_2$, one finds

$$\Theta = 2 \arcsin y \left[1 - 4(k + n)y^2 + 16 \ kny^4 \right]^{-\frac{1}{2}} . \quad (3)$$

Equation (3) also reduces to (1) with $h = k + n$ for small values of y, but curves over less rapidly than (1) and so cannot fit the data, at least in our particular case.
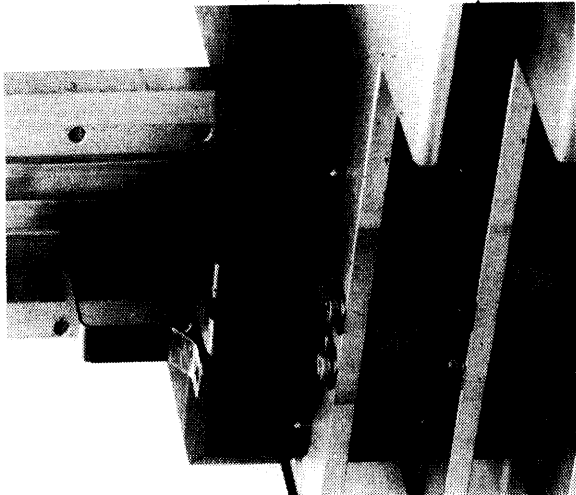
Fig. 5 - Coupling loops
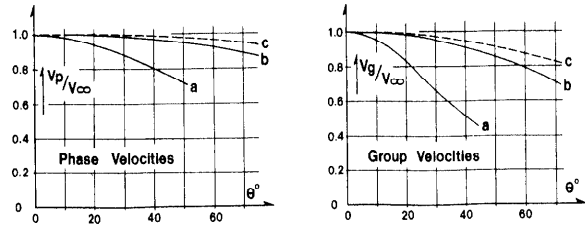
Fig. 6 - a) Original, b) Modified, c) LC line

To gain further insight into the role of the mutual inductance, a series of metal septa were next introduced across the kicker aperture, thus practically eliminating the coupling between cells. This gave the dispersion curve of Fig. 2(d).

We conclude that L_2 has some physical reality, but that for the kicker measured, a major part of it is a circuit representation of the mutual inductance between adjacent cells.

Improved kicker

The apparent importance of the mutual inductance suggested that it might be possible to improve the performance by deliberately coupling successive cells.

To do this, part of the "hot" conductor was milled away and the capacity plates modified to permit the introduction of loops coupling successive ferrite backlegs to each other in the desired polarity (Fig. 5). It was found possible to provide quite reasonable clearances in relation to the fields expected in high-power operation.

From a circuit point of view this arrangement is equivalent to introducing a negative inductance in series with the shunt elements. This resulted in a very marked improvement, Fig. 2(b). For comparison, the curve for an LC line is also shown in Fig. 2(c).

The corresponding phase and group velocities normalized to their value V_∞ for infinite wavelength are shown in Fig. 6.

Pulse measurement

We now compare the pulse behaviour of the original kicker to that of the same structure with the coupling loops.

Figure 7 shows the voltage pulse at the entrance and exit of a kicker, a) for the original and b) for the modified structure.

a)   b)
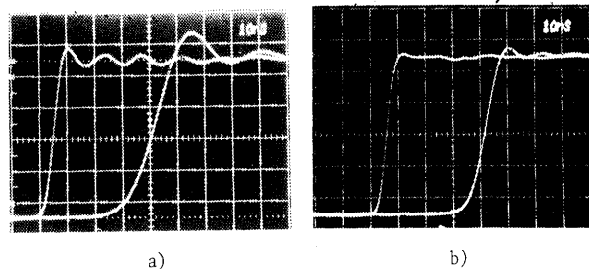
Fig. 7 - Voltage propagation

Figure 8 gives a similar comparison for the current pulse, obtained by measuring the rise of the magnetic field in the first and last cell of the kicker.

Figure 9 shows the rate of change of the magnetic flux $\dot{\Phi}$ and the flux Φ. The asymmetry of $\dot{\Phi}$ for the original kicker is much greater than for the improved structure. The change for Φ is not so striking but is still clearly visible (Fig. 10).

a)   b)
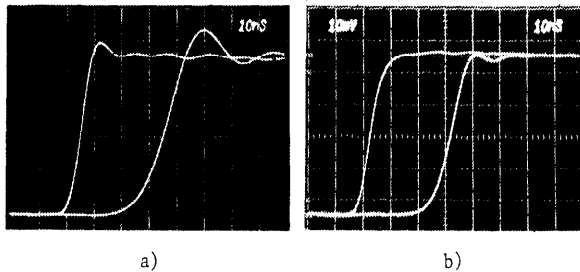
Fig. 8 - Current pulse propagation

a)   b)
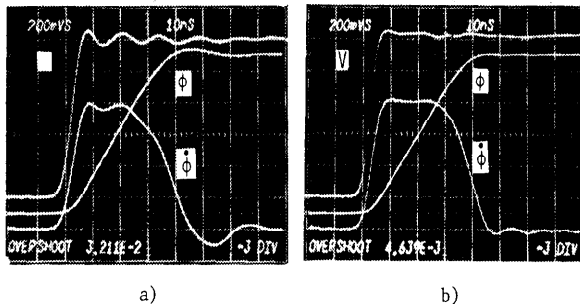
Fig. 9 - Voltage pulse V, rate of rise of flux $\dot{\Phi}$ and flux Φ
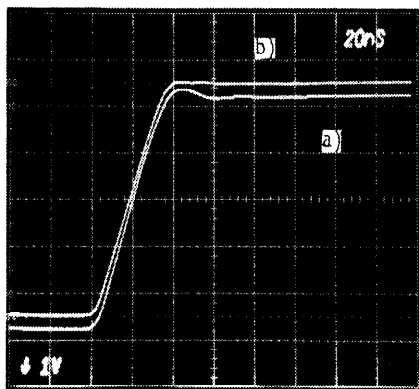
Fig. 10 - Comparison of rise of kick strength for
a) original and b) modified magnets

Conclusion

The propagation characteristics of a travelling wave kicker can be substantially improved by introducing inductive coupling between successive cells.

Apart from the loops described, this may possibly be done by other means, such as distorting the cells.

By extending the linear region of the dispersion curve, it appears possible to use fewer cells for a given performance and obtain more freedom to design kickers with low characteristic impedance.

Appendix

Reduction of measurement errors through the use of a digital processing oscilloscope (DPO).

The pulse measurements of the total kicker flux were done using a loop formed by a 50 Ω line, shorted at one end. This type of measurement suffers from two main difficulties[6]:

i) there is an unwanted capacitive signal, which adds to or subtracts from the desired magnetic signal, depending on the orientation of the loop;

ii) depending on the relative direction of the waves in the kicker and along the loop, the magnetic signal is lengthened or shortened by the loop transit time, and in addition the shape of the kicker flux rise is incorrectly reproduced.

Both these effects can be much reduced or eliminated by using a DPO.

As regards (i), the signals for two loop orientations are stored and then subtracted. To the extent that the capacitive interference is independent of loop orientation, it is thus eliminated.

As a verification Fig. A.1, upper trace, shows half the algebraic sum of two loop signals, thus eliminating the magnetic signal, while the lower trace shows the signal from a loop at 90° to the magnetic field. The similarity of the two traces confirms that the capacitive signal is substantially independent of loop orientation.
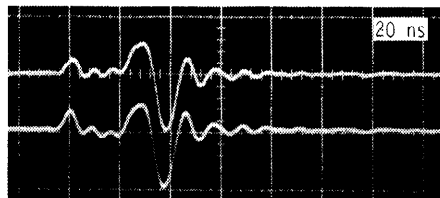
Fig. A.1

As regards (ii), all loop transit time effects can be reduced to negligible proportions by using a loop only a fraction (here 1/3) of the length of the kicker. Signals from the short loop in successive positions are summed by the DPO in their correct time relation and then integrated. The $\dot{\Phi}$ traces shown are in fact the sum of six measurements (2 orientations × 3 positions).

References

1. A. Brückner, A non-linear step-pulse steepening delay line, CERN 68-25 (1968).

2. A. Brücker, Kicking protons, fast and cheap, Proc. US Particle Accelerator Conf., Chicago, 1971 IEEE Trans. Nucl. Sci. NS-18, 976 (1971).

3. P.G. Innocenti, B. Kuiper, A. Messina and H. Riege, On the design of "Fast kicker" magnets, Proc. 3rd Internat. Conf. on Magnet Technology, Hamburg, 1970 (DESY Hamburg, 1970), p. 559.

4. D. Fiander, Hardware for a full aperture kicker system for the CPS, Proc. US Particle Accelerator Conf., Chicago, 1971, IEEE Trans. Nucl. Sci. NS-18 1022 (1971).

5. D. Fiander, D. Grier, K. Metzmatcher, P. Pearce, A replacement transfer injection kicker, PS/AE/Note 76-13.

6. D. Fiander, Private communication.